

# Coupling of benthic oxygen uptake and silica release: implications for estimating biogenic particle fluxes to the seafloor

Katherina Seiter · Christian Hensen · Matthias Zabel

Received: 16 March 2010 / Accepted: 31 March 2010 / Published online: 20 April 2010  
© Springer-Verlag 2010

**Abstract** A new approach to predict biogenic particle fluxes to the seafloor is presented, which is based on diffusive oxygen uptake and, in particular, opal fluxes to the seafloor. For this purpose, we used a recently published empirical equation coupling benthic silica to oxygen fluxes, and showing a clear negative correlation between Si and O<sub>2</sub> fluxes. Dissolution of biogenic silica mediated by aerobic microbial activity has been inferred at 24 sites along the African and South American continental margins. Based on the assumption that these findings hold essentially for the entire Southern Atlantic Ocean, we applied the silica to oxygen flux ratio to a basin-wide grid of diffusive oxygen uptake extracted from the literature. Assuming that the silica release across the sediment-water interface equals the particulate flux of biogenic opal to the seafloor, we estimated minimum opal rain rates. We combined these calculations with published relationships between aerobic organic carbon mineralization and dissolution rates of calcite above the hydrographical lysocline, thereby assessing the calcite rain rate and particulate organic carbon flux to the seafloor. The addition of the buried fraction

completes our budget of biogenic particulate rain fluxes. The combination of such empirical equations provides a powerful and convenient tool which greatly facilitates future investigations of biogenic particle fluxes to the seafloor.

## Introduction

Net primary production acts as a sink for surface-water CO<sub>2</sub> in the ocean. A certain fraction of the particulate material sinks out of the euphotic zone as export production, thereby efficiently removing biogenic components such as calcium carbonate, opal and organic carbon from the sea surface. Particle flux rates and the type of exported biogenic material are tightly controlled by nutrient supply to surface waters as well as oceanographic boundary conditions (e.g. Ganachaud and Wunsch 2002). Subsequently, these particles are largely remineralized and only a small fraction is buried in the sediments. A thorough understanding of the turnover of biologically active elements, known as the “biological pump”, is key to our perception of global climate change and, for example, its vulnerability to anthropogenic eutrophication along continental margins. Despite substantial improvements in this field of study, major uncertainties exist with respect to the coupling of Si and C cycles (Ragueneau et al. 2006), the global calcium carbonate budget and calcium carbonate dissolution within the supersaturated mesopelagic zone (Berelson et al. 2007; Honjo et al. 2008), and the controls of export mechanisms leading to spatial and temporal variations (Kemp et al. 2006; Ragueneau et al. 2006; Lampitt et al. 2009).

In general, the behaviour of opal in the ocean, including its formation and recycling, and its sedimentation and dissolution in the water column, has many analogies to that

---

K. Seiter (✉)  
GDfB—Geological Service for Bremen,  
Leobener Str,  
28359 Bremen, Germany  
e-mail: kseiter@gdfb.de

M. Zabel  
MARUM—Center for Marine Environmental Science, University  
of Bremen,  
P.O. Box 330440, 28359 Bremen, Germany

C. Hensen  
Leibniz-Institute of Marine Sciences,  
IFM-GEOMAR, Marine Biogeochemistry,  
Wischhofstr. 1-3,  
24148 Kiel, Germany

of organic matter (e.g. Brzezinski 1985; Nelson et al. 1995; Tréguer et al. 1995; Ragueneau et al. 2000). Under conditions of enhanced nutrient supply to surface waters, promoting diatom growth, biogenic opal production can account for 35–75% of primary production (PP), equivalent to 200–280 Tmol Si year<sup>-1</sup> in the world oceans (Nelson et al. 1995; Tréguer et al. 1995). Once these and other organisms die, organic matter degradation proceeds rapidly. Most organic matter remineralization occurs already in the upper water column. The latest calculations of carbon export production in the global ocean accounts for approx. 20–25% of global PP, which amounts to 47.5 Gt C year<sup>-1</sup> (Behrenfeld and Falkowski 1997; Schlitzer 2002). About 1–1.5% of organic compounds produced in the surface waters of the deep sea reaches the seafloor (e.g. Berger et al. 1989; Wollast 1998; Christensen 2000; Antia et al. 2001; Schlitzer 2002; Seiter et al. 2005), but less than 0.01% eventually becomes buried in the sediments. Thus, 99% of surface production is decomposed by microbial activity in the water column. For biogenic opal, several budgets have appeared in the literature since the 1990s (e.g. Nelson et al. 1995; Tréguer et al. 1995; Ganachaud and Wunsch 2002; Ridgwell et al. 2002). Most authors agree that relative amounts of opal export production and buried opal from surface production are about 50 and 2.5% respectively. Latest estimates predicted by the model of Ridgwell et al. (2002) confirmed these budgets, but differed in the partitioning of silica dissolution between the water column and surface sediments. Compared to the values proposed by Tréguer et al. (1995), Ridgwell et al. (2002) halved the amount of silica remineralized in the water column (cf. 48.1 vs. 90.9 Tmol Si year<sup>-1</sup>), but increased the silica rain rate to the seafloor by a factor of 4 (cf. 83.2 vs. 23 Tmol Si year<sup>-1</sup>). Evidently, the biogenic opal rain rate and burial efficiency could be about one order of magnitude higher than that of organic carbon. Results of Moriceau et al. (2007a) show that the silica rain rate is mainly controlled by particle formation which enhances rapid sinking to the seafloor and prevents early remineralization in the surface water. This effect is obviously amplified by significantly lower specific dissolution rates for aggregated diatom frustules, compared to dissolution rates for freely suspended diatoms (Moriceau et al. 2007b). Nevertheless, existing uncertainties about opal rain rates and burial efficiency illustrate the key importance of the benthic boundary layer for a better assessment of the oceanic silica budget (e.g. Thomsen 2003).

Despite the differences in recycling intensity, there are several aspects suggesting an ocean-dependent coupling between organic carbon and biogenic silica in the water column (Ragueneau et al. 2000), where the respective dissolution processes result in comparable flux relations. Silicate, an essential nutrient for the planktonic community,

is dissolved in the sediment depending on the degree of undersaturation. This state of thermodynamic imbalance is generally seen as the main controlling factor of biogenic silica dissolution (e.g. Tréguer et al. 1995; Rabouille et al. 1997). Nevertheless, some studies have provided evidence that bacterial abundance and activity can also play an important role in the dissolution rate of diatom frustules (Aller and Aller 1998; Bidle and Azam 1999; Bidle et al. 2003). Aller and Aller (1998) concluded that biogenic housing increases the surface area to maintain a rapid supply of electron acceptors. The macrofauna grazes on microbes, which stimulates production. Metabolites inhibiting microbial activity are rapidly removed through irrigated burrows, but also the microbial activity itself interferes with the relation between organic carbon degradation and opal dissolution (Bidle and Azam 1999; Bidle et al. 2003). Bacterial ectoprotease action on marine diatom detritus strongly accelerates silica dissolution rates, by the removal of organic coatings which protect frustules from being directly exposed to undersaturated seawater.

Holstein and Hensen (2010) investigated pore-water profiles in South Atlantic sediments. They detected a correlation between benthic oxygen uptake and dissolved silica release, which suggests the existence of microbial dissolution of biogenic opal with a depth-independent stoichiometry of 0.52. These authors based their interpretation on aerobic microbial respiration, which controls the dissolution of biogenic silica in marine sediments by means of an enzymatic removal of protective coatings from diatom skeletons (Aller and Aller 1998; Bidle and Azam 1999; Bidle et al. 2003).

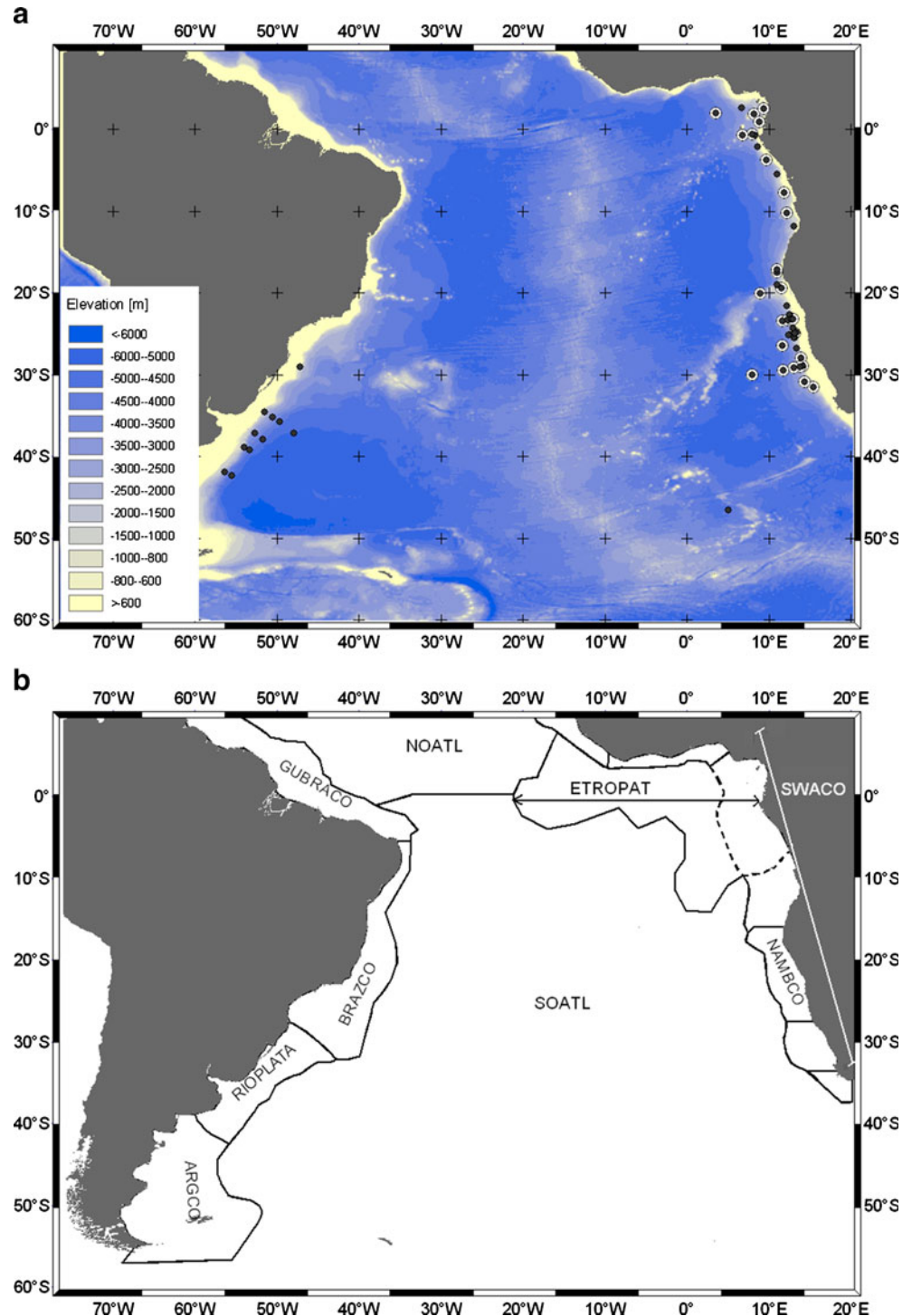
Extrapolating this coupling of local data to the South Atlantic can provide new prospects in estimating regional benthic silica fluxes (e.g. Hensen et al. 1998; Zabel et al. 1998). Moreover, it would permit the regionalization of the particulate flux of biogenic opal to the sediment. Conventionally, the amount of particles actually reaching the seafloor is deduced from sediment trap measurements, or by calculating accumulation rates. However, the database derived from trap investigations is sparse and often affected by the lateral transport of suspended matter, a major regional uncertainty. Estimates based on accumulation rates record only the fraction preserved within the sediments, and are strongly affected by the uncertainties in current age models. By contrast, benthic biogeochemical mineralization rates are closely coupled with the availability of labile organic carbon components as the main controlling factor, and can be interpreted as a proxy for the particle input or, more precisely, its mineralized fraction (Jahnke 1996; Wenzhoefer and Glud 2002; Seiter et al. 2005). Due to complex interrelations catalyzed mostly by microbes, such an approach is not restricted to the rain rate of organic debris. For example, the degradation of organic carbon is

also an important process driving the dissolution of calcite in surface sediments above the hydrographical lysocline (e.g. Pfeifer et al. 2002). Our investigation, which uses aerobic respiration as a proxy, opens new ways of predicting particulate biogenic particle flux to the seafloor. In this regard, we provide a new platform for further efforts to facilitate the regionalization process of benthic fluxes and global biogeochemical budgets.

### Study area and benthic provinces

This study focuses on the tropical and subtropical Southern Atlantic Ocean basin between 10°N and 50°S. The total investigated area, excluding the <1,000 m water depth zone off the coastline, amounts to about  $3.7 \times 10^{13} \text{ m}^2$  (Fig. 1a). In general, the surface and subsurface water circulation, dominated by a subtropical gyre, controls PP distribution

**Fig. 1** **a** Study area and core locations (dots). The black and underlying white dots indicate locations of geochemical investigations (Tables 2 and 3). White dots Silica and oxygen flux rates ( $J_{Si \text{ mod.}}$  and  $J_{O_2 \text{ mod.}}$ ) used in the modelling of  $R_{Si/O_2}$  (extracted from Holstein and Hensen 2010), black dots comparative benthic flux data calculated for the present study. We used the ETOPO 2–2 min Global Relief provided by the National Geophysical Data Center (NGDC, Boulder, CO) to draw the bathymetry map. **b** Benthic TOC-based provinces (extracted from Seiter et al. 2004; see text for explanation of province names)



patterns as the major source of biogenic particles in sediments.

As a whole, the Southern Atlantic is an oligotrophic ocean, with moderate PP in the central gyre region and enhanced phytoplankton growth in the coastal and equatorial upwelling regions (e.g. Wefer and Fischer 1993; Shannon and Nelson 1996; Antoine et al. 1996). Driven by the trade winds, the surface currents induce a coastal and open ocean upwelling of nutrient-rich water masses. In the following, we apply the subdivision of benthic provinces of Seiter et al. (2004; Fig. 1b, Table 1), based on province-specific sedimentary regimes.

The equatorial upwelling region is located in the benthic province ETROPAT (mean PP of  $182 \text{ g C m}^{-2} \text{ year}^{-1}$ , based on Antoine et al. 1996; Table 1, Fig. 1b). Coastal upwelling occurs mainly in the south-eastern Atlantic provinces NAMBCO and SWACO between  $30^\circ\text{N}$  and  $15^\circ\text{S}$  (mean PP of  $225\text{--}256 \text{ g C m}^{-2} \text{ year}^{-1}$ , Shannon and Nelson 1996). High productivity is fostered by the riverine nutrient discharges of the Ougoue River at about  $0.5^\circ\text{S}$  and of the Congo River at  $6^\circ\text{S}$ . Here, bulk terrigenous organic matter has been estimated to constitute 58–76% of the marine benthic total organic carbon (TOC) pool. Substantial amounts of low-reactivity, mature organic matter (plant debris) have been found as far offshore as the distal base of the Congo deep-sea fan (Wagner et al. 2004). Enhanced PP is known also from the continental margin off Argentina and Brazil (e.g. the ARGCO province,  $140 \text{ g C m}^{-2} \text{ year}^{-1}$ ), associated with the confluence zone of the Malvinas and Brazil currents.

With the exception of the opal belt around Antarctica (e.g. DeMaster 1981), biogenic sedimentation above the hydrographical lysocline in the Southern Atlantic Ocean is predominantly calcareous. Nevertheless, an area showing high accumulation rates of amorphous silica has been documented

off the Congo River mouth, where up to 40% of the sediment consists of biogenic opal (van der Gaast and Jansen 1984).

## Materials and methods

### Geochemical raw data sources and modelled data

The present study draws upon a negative linear correlation between silica and oxygen flux rates, based on the assumption that respiration related to aerobic microbial activity is the dominant process controlling the biogenic dissolution of silica (Holstein and Hensen 2010). Experimental benthic silica flux profiles were generated by the application of a depth-independent stoichiometry of silica to oxygen flux rates ( $R_{\text{Si}/\text{O}_2}$ , Eq. 1, Holstein and Hensen 2010):

$$J_{\text{Si mod.}} = -R_{\text{Si}/\text{O}_2} \times J_{\text{O}_2 \text{ mod.}} \quad (1)$$

where the calculated  $R_{\text{Si}/\text{O}_2}=0.52$  of modelled fluxes (cf. positive coupling coefficient of  $J_{\text{Si mod.}}$  to  $J_{\text{O}_2 \text{ mod.}}$ ) has a standard deviation (SD) of 0.14 with values varying from 0.3 to 0.9 ( $n=24$ ).

Equation (1) is based on a published dataset of pore-water and sediment samples retrieved by multicorer at 24 locations during five cruises aboard the RV *Meteor* (M29/1, M34/2, M38/2, M41/1 and M46/2) in the Southern Atlantic Ocean during the period 1994–1999. The data were collected along the continental margins off South Africa, especially Namibia and Angola, and off the coasts of Argentina, Uruguay, southern Brazil, and at one location off the coast of northern Brazil. In situ measurements were also carried out at several core locations ( $n=17$  of 24).

Two types of datasets were used in the present study. One dataset (described above) includes modelled  $J_{\text{Si}}$  and

**Table 1** Mean contents of opal, calcite and total organic carbon (TOC) in surface sediments of South Atlantic provinces, extracted as mean and maximum values of processed grids from Seiter et al.

Province <sup>a</sup>	Max. opal (dry wt%)	Mean opal	Max. calcite	Mean calcite	Max. TOC	Mean TOC	Max. PP ( $\text{g m}^{-2} \text{ year}^{-1}$ )	Mean PP
SOATL	89	13.0	106	34	1.7	0.4	360	101
NAMBCO	41	3.7	85	67	8.2	2.7	562	256
SWACO	41	6.8	93	39	8.2	1.5	1,159	225
ETROPAT	28	13.0	96	48	3.5	0.7	1,159	182
GUI	23	6.8	46	11	2.1	1.1	819	189
ARGCO	24	2.6	69	30	0.8	0.3	557	140
RIOPLATA	16	4.8	13	3	3.4	0.8	1,210	178
GUBRACO	21	1.8	75	49	1.0	0.4	1,280	193
BRAZCO	20	3.6	84	46	1.1	0.5	381	128

<sup>a</sup> SOATL Southern Atlantic Ocean; NAMBCO Benguela upwelling province off Namibia; SWACO SW African continental margin, including NAMBCO; ARGCO continental margin off Argentina; RIOPLATA off Rio de la Plata mouth, N Argentina/Uruguay; BRAZCO continental margin off Brazil; GUBRACO continental margin off N Brazil and Guyana

(2004). Corresponding mean and maximum primary production (PP) were recalculated by Seiter et al. (2005), after Antoine et al. (1996). Geographical positions of provinces are shown in Fig. 1b

$J_{O_2}$  data, and corresponding calculated fluxes based on the conventional method of fitting experimental benthic silica flux profiles in an exponential approach ( $n=24$ ), after Sayles et al. (1996). This dataset (Table 2), derived from Holstein and Hensen (2010), represents the basis for further calculations in this study. An additional dataset (Table 3) of exponentially recalculated fluxes ( $n=24$ ) was taken from pore-water data published by Hensen et al. (1998) and Zabel et al. (1998). The combined dataset ( $n=48$  data points) was used to examine the quality of the processed distribution patterns of benthic silica fluxes and associated biogenic particle fluxes.

**Table 2** Core sites ( $n=24$ ), water depths, comparison of benthic fluxes of oxygen and silica, modelled and fitted exponentially by Holstein and Hensen (2010), ratios of modelled benthic silica vs.

The various types of fluxes for  $J_{Si}$  or  $J_{O_2}$  are termed as follows: exponentially calculated fluxes (Sayles et al. 1996) are called  $J_{Si\ exp.}$  or  $J_{O_2\ exp.}$ . We used  $J_{Si\ mod.}$  or  $J_{O_2\ mod.}$  for model fluxes. Values derived from the generated grids are termed  $J_{Si\ grid}$  or  $J_{O_2\ grid}$ .

Methods of measurements and sampling devices are described in the references cited above. For more information on the analytical procedures, the reader is referred to Gundersen and Jørgensen (1990), Glud et al. (1994), Zabel et al. (1998) and Wenzhoefer et al. (2001). Modelling procedures are described in Holstein and Hensen (2010).

oxygen,  $R_{Si/O_2}$ , calculated after Holstein and Hensen (2010), and gridded silica fluxes (this study; *n.v.* not validated)

Core no.	Longitude	Latitude	Water depth	$J_{Si\ exp.}^a$	$J_{Si\ mod.}^b$	$J_{O_2\ exp.}^a$	$J_{O_2\ emod.}^b$	$R_{Si/O_2}^c$	$J_{Si\ grid}^d$
			(m)	(mol m <sup>-2</sup> year <sup>-1</sup> )					(mol m <sup>-2</sup> year <sup>-1</sup> )
Cruise M46/2									
GeoB 6202	47.1700 W	29.087 S	1,497	0.08	0.07	-0.22	-0.23	0.30	0.13
GeoB 6214	51.4430 W	34.5250 S	1,566	0.17	0.17	-0.40	-0.39	0.44	0.21
GeoB 6219	50.5650 W	35.1860 S	3,551	0.17	0.15	-0.29	-0.30	0.50	0.17
GeoB 6223	49.6810 W	35.7400 S	4,280	0.11	0.18	-0.29	-0.41	0.44	0.13
GeoB 6226	47.8990 W	37.1580 S	5,055	0.11	0.10	-0.22	-0.21	0.48	0.13
GeoB 6229	52.6500 W	37.2070 S	3,442	0.24	0.23	-0.50	-0.47	0.49	0.24
GeoB 6230	51.6900 W	37.8950 S	4,381	0.34	0.43	-0.58	-0.82	0.52	0.16
Cruise M41/1									
GeoB 4906	8.3783E	0.6900 S	1,272	0.31	0.46	-0.82	-0.81	0.57	0.26
GeoB 4909	8.6250E	2.0683 S	1,305	0.21	0.25	-0.51	-0.50	0.50	0.18
GeoB 4913	11.0717E	5.5033 S	1,296	0.40	0.53	-0.96	-0.95	0.56	0.54
GeoB 4917	13.0733E	11.9033 S	1,300	0.23	0.30	-0.99	-0.98	0.31	n.v.
GeoB 4901	6.7200E	2.6820 N	2,177	0.17	0.21	-0.26	-0.33	0.64	0.27
Cruise M38/2									
GeoB 4417	5.1383E	46.5750 S	3,511	0.08	0.05	-0.14	-0.08	0.63	0.09
Cruise M34/2									
GeoB 3702	13.4550E	26.7917 S	1,319	0.99	0.95	-1.36	-1.35	0.70	0.42
GeoB 3703	13.2317E	25.5167 S	1,376	0.87	0.90	-1.86	-1.38	0.65	0.50
GeoB 3705	12.9967E	24.3033 S	1,305	0.59	0.66	-1.54	-1.24	0.53	0.44
GeoB 3706	12.6017E	22.7167 S	1,313	0.45	0.49	-1.19	-1.19	0.41	0.29
GeoB 3707	12.1933E	21.6250 S	1,350	0.50	0.54	-0.88	-0.83	0.65	0.49
GeoB 3715	11.0567E	18.9550 S	1,204	0.66	1.01	-1.15	-1.13	0.89	0.52
GeoB 3719	11.0567E	18.9550 S	1,995	0.46	0.55	-1.04	-0.96	0.58	0.43
Cruise M29/1									
GeoB 2704	53.9283 W	38.9250 S	3,247	0.31	0.46	-1.15	-0.88	0.43	0.15
GeoB 2705	53.3633 W	39.2433 S	4,474	0.28	0.47	-0.96	-0.88	0.53	0.16
GeoB 2706	55.5350 W	42.3683 S	4,700	0.22	0.33	-0.85	-0.74	0.45	0.12
GeoB 2707	56.3233 W	41.9450 S	3,167	0.21	0.23	-0.78	-0.78	0.30	0.09

<sup>a</sup> Exponentially calculated fluxes extracted from Holstein and Hensen (2010); in situ data are indicated in *italics*

<sup>b</sup> Modelled fluxes extracted from Holstein and Hensen (2010)

<sup>c</sup>  $R = J_{Si}/J_{O_2}$ , positive coupling coefficient (Eq. 1), based on modelled fluxes (extracted from Holstein and Hensen 2010)

<sup>d</sup> Gridded silica fluxes (this study)

**Table 3** Benthic silica fluxes refitted exponentially for this study using pore-water data published by Hensen et al. (1998) and Zabel et al. (1998), and corresponding gridded silica fluxes derived from the generated regular silica flux grid ( $n=24$ , this study)

Core no.	Longitude	Latitude	Elevation (m)	$J_{Si \text{ exp.}}^a$ (mol m <sup>-2</sup> year <sup>-1</sup> )	$J_{Si \text{ grid.}}^b$
GeoB 1701	3.5500E	1.9500 N	4,162	0.10	0.09
GeoB 1703	11.0167E	17.4533 S	1,771	0.51	0.56
GeoB 1708	8.9667E	20.0967 S	2,321	0.10	0.10
GeoB 1710	11.6900E	23.4300 S	2,988	0.23	0.16
GeoB 1711	12.3733E	23.3167 S	1,928	0.15	0.27
GeoB 1712	12.8050E	23.2533 S	1,004	0.24	0.27
GeoB 1715	11.6383E	26.4700 S	4,095	0.18	0.12
GeoB 1716	14.0033E	27.9517 S	1,510	0.12	0.28
GeoB 1719	14.1733E	28.9267 S	1,023	0.15	0.31
GeoB 1720	13.8367E	28.9983 S	2,004	0.12	0.24
GeoB 1721	13.0900E	29.1733 S	3,045	0.07	0.09
GeoB 1722	11.7500E	29.4500 S	3,974	0.06	0.08
GeoB 1724	8.0417E	29.9717 S	5,102	0.05	0.11
GeoB 2004	14.3467E	30.8683 S	2,571	0.12	0.31
GeoB 3714	10.9983E	17.1600 S	2,060	0.36	0.52
GeoB 3718	13.1600E	24.8950 S	1,316	0.64	0.47
GeoB 4903	8.1700E	1.9167 N	2,385	0.12	0.23
GeoB 4904	8.8800E	0.9617 N	1,349	0.31	0.31
GeoB 4905	9.3900E	2.5000 N	1,328	0.54	0.25
GeoB 4907	8.0267E	0.6250 S	2,066	0.13	0.25
GeoB 4908	6.8383E	0.7133 S	3,028	0.12	0.16
GeoB 4912	9.7850E	3.7300 S	1,298	0.20	0.35
GeoB 4915	11.8733E	7.7500 S	1,306	0.21	0.38
GeoB 4916	12.2068E	10.1733 S	1,294	0.18	0.39

<sup>a</sup> Exponentially calculated fluxes (this study; flux calculation method after Sayles et al. 1996)

<sup>b</sup> Gridded fluxes (this study)

### Estimation of biogenic particulate fluxes

Benthic biogeochemical transfer rates are closely coupled with the availability of labile organic carbon components. Thus, the main controlling factor, i.e. benthic aerobic respiration, can be interpreted as a proxy for the minimum inputs of biogenic particulate components ( $J_{P \text{ min.}}$ ), such as calcite, opal and organic carbon or, rather, their aerobically mineralized fractions (Jahnke 1996; Wenzhoefer and Glud 2002; Pfeifer et al. 2002; Seiter et al. 2005):

$$J_{P \text{ min.}} = M_{\text{opal}} \times |J_{\text{Si}}| + M_{\text{CaCO}_3} \times |J_{\text{Ca}}| + M_{\text{OC}} \times |J_{\text{OC}}| \quad (2)$$

where  $|J|$  is the minimum flux of the mineralized fraction of a given biogenic component, in units of mol m<sup>-2</sup> year<sup>-1</sup>,  $M$  the molar mass (g mol<sup>-1</sup>) of opal (SiO<sub>2</sub>), calcite (CaCO<sub>3</sub>) and organic carbon (OC), and  $J_{P \text{ min.}}$  the minimum flux of particulate opal, calcite and organic carbon to the seafloor, calculated in units of g m<sup>-2</sup> year<sup>-1</sup>.

Calcite fluxes ( $J_{\text{Ca}}$ ) are expressed by calcite dissolution rates ( $DR_{\text{CaCO}_3}$ ), and the linear correlation between calcite dissolution rates and the aerobic mineralization of organic

carbon shown in Eq. (3), after Pfeifer et al. (2002). This relationship is valid above the hydrographical calcite lysocline (Pfeifer et al. 2002). The aerobic turnover of organic carbon is expressed as diffusive oxygen uptake or oxygen flux rate,  $J_{\text{O}_2}$ , with a molecular C:O<sub>2</sub> ratio of 106:138 (Redfield 1958; Froelich et al. 1979):

$$|J_{\text{Ca}}| = DR_{\text{CaCO}_3} = 1.1 \times \frac{106}{138} \times |J_{\text{O}_2}| - \frac{9.3}{100} \quad (3)$$

where  $DR_{\text{CaCO}_3}$  and  $J_{\text{O}_2}$  have the units mol m<sup>-2</sup> year<sup>-1</sup>.

Based on Eq. (2), we estimated  $J_{P \text{ min.}}$  by substituting  $|J_{\text{Si}}|$  and  $|J_{\text{Ca}}|$  in Eq. (2) with  $J_{\text{Si mod.}}$  of Eq. (1) and  $J_{\text{Ca}}$  of Eq. (3) respectively. The organic carbon flux ( $J_{\text{OC}}$ ) is substituted by the aerobic respiration rate (after Froelich et al. 1979):

$$J_{P \text{ min.}} = M_{\text{opal}} \times 0.52 \times |J_{\text{O}_2}| + M_{\text{CaCO}_3} \times \left( 1.1 \times \frac{106}{138} \times |J_{\text{O}_2}| - \frac{9.3}{100} \right) + M_{\text{OC}} \times \frac{106}{138} \times |J_{\text{O}_2}| \quad (4)$$

Equation (4) can be simplified to

$$J_{P \text{ min.}} = A_1 \times |J_{O_2}| + (A_2 \times |J_{O_2}| - 9.3) \wedge \Delta CO_3^{2-} < 0 \quad (5)$$

In these two equations,  $M$  is the molecular mass in  $\text{g mol}^{-1}$ ,  $J_{P \text{ min.}}$  is in  $\text{g m}^{-2}\text{year}^{-1}$ ,  $J_{O_2}$  in  $\text{mol m}^{-2}\text{year}^{-1}$ , and  $A_1$  and  $A_2$  are constants amounting to 41.1 and 84.6  $\text{g mol}^{-1}$  respectively.

The term in parenthesis in Eq. (5) represents the particulate calcite component and is set to zero below the hydrographical lysocline, defined by the saturation state  $\Delta CO_3^{2-}$  as the difference between the  $CO_3^{2-}$  concentration of calcite saturation and the in situ  $CO_3^{2-}$  concentration of water masses (cf. Archer 1996).

In the open Southern Atlantic Ocean, there are no pronounced differences between the total biogenic particulate rain to the seafloor and the calculated minimum particle flux of biogenic components ( $J_{P \text{ tot.}} \approx J_{P \text{ min.}}$ ) but, along the continental margins,  $J_{P \text{ min.}}$  may be significantly lower than the total biogenic particulate flux. The additional input of marine and terrestrial biogenic material from the shallow-water areas can be expressed by increased burial rates, which are accounted for in Eq. (6). Burial rates ( $\beta$ ) were calculated after van Andel (1975):

$$J_{P \text{ tot.}} = J_{P \text{ min.}} + \beta \quad \text{where} \quad (6)$$

$$\beta = 0.1 \times PC \times SR \times DBD$$

in which PC is the relative content of sedimentary particulate biogenic components ( $\text{g } 100 \text{ g}^{-1}$ ), DBD the dry bulk density ( $\text{g cm}^{-3}$ ) and SR the sedimentation rate ( $\text{cm } 1,000 \text{ year}^{-1}$ ), with  $\beta$  and  $J_{P \text{ tot.}}$  having the units  $\text{g m}^{-2}\text{year}^{-1}$ .

#### Regionalization and budgeting of benthic silica and biogenic fluxes

To extrapolate the silica fluxes at a basin-wide scale,  $J_{Si \text{ grid}}$ , a regular basin-wide grid of diffusive benthic oxygen fluxes at a  $1^\circ$  grid point resolution,  $J_{O_2 \text{ grid}}$ , was extracted from Seiter et al. (2005), and  $R_{Si/O_2}$  (cf. Eq. 1) was applied to this grid. The biogenic particle fluxes were generated in an analogous manner, applying Eq. (5) to calculate the mineralized fraction,  $J_{P \text{ min. grid}}$ , and Eq. (6) to process the total fraction,  $J_{P \text{ tot. grid}}$ , on the regular distribution pattern of  $J_{O_2 \text{ grid}}$  (Seiter et al. 2005).

Calculation of the basin-wide budgets within the benthic provinces was done after Seiter et al. (2004), projecting the appropriate distribution patterns in a Lambert azimuthal equal-area projection. The general map and budgeting is presented at a  $1^\circ$  grid point resolution. The required resampling of the cells of the metric system ( $\text{m}^2$ ) was done by bilinear interpolation of the cell values (ArcGIS 9.1, ESRI®).

Sedimentation rates and dry bulk density values were extracted from regular distribution patterns of SR and DBD at  $1^\circ$  grid point resolution (after Mollenhauer et al. 2002). Sedimentary contents of opal, calcite and TOC in surface sediments of the various provinces were extracted from calculated distribution patterns of these sedimentary components, underlain by a regular matrix of  $1^\circ$  grid point resolution according to Seiter et al. (2004). The corresponding mean and maximum PP were extracted from recalculations made by Seiter et al. (2004) based on Antoine et al. (1996; Table 1). The position of the hydrographical lysocline was calculated from a  $2^\circ$  grid point matrix of bottom-water  $\Delta CO_3^{2-}$  data (after Archer 1996).

## Results

### Extrapolation of silica flux rates to a basin-wide scale

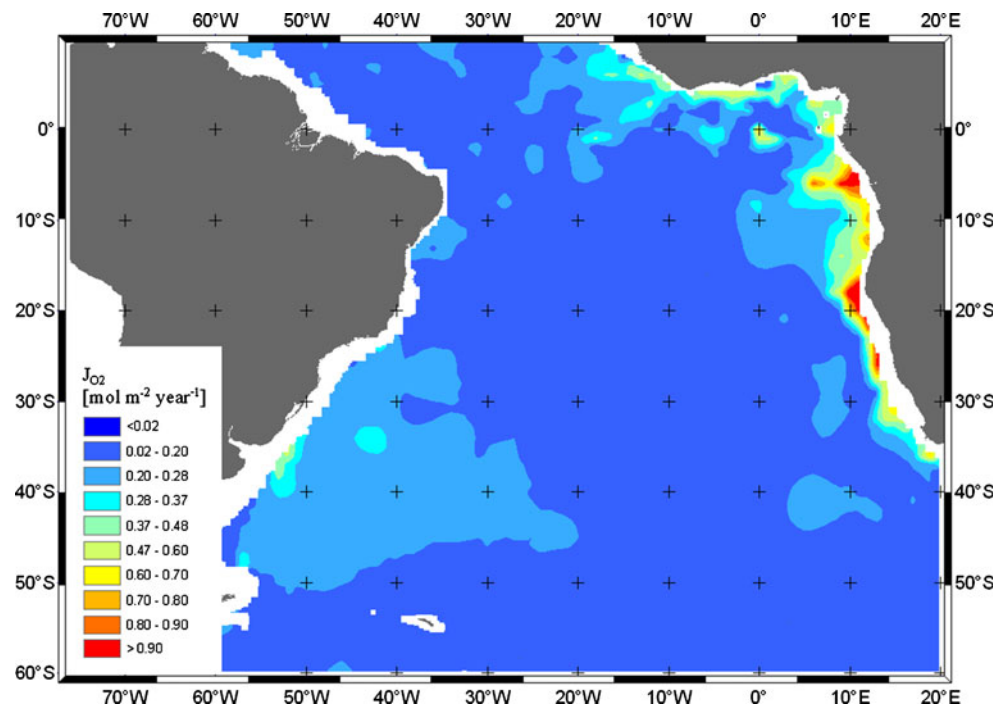
As expected, the basin-wide silica flux ( $J_{Si \text{ grid}}$ ) distribution pattern is comparable to the  $J_{O_2 \text{ grid}}$  distribution map of Seiter et al. (2005), shown in Fig. 2. Highest fluxes are observed along the continental margins. Despite some spatial variations, a general decrease with water depth is detected. This pattern generally agrees with former estimations made by Hensen et al. (1998) and Zabel et al. (1998). In contrast to lower estimations reported by Hensen et al. (1998), considerably higher  $J_{Si \text{ grid}}$  values offshore of the Congo River mouth have been calculated in the present study. The highest  $J_{Si \text{ grid}}$  values (max. of  $0.62 \text{ mol m}^{-2}\text{year}^{-1}$ ) occur in the upwelling region along the continental margin off Namibia (Fig. 3).

The Argentine Basin is a heterogeneous region, displaying lowest release rates (smaller than  $0.1 \text{ mol m}^{-2}\text{year}^{-1}$ ) in the southern part and higher values (up to  $0.3 \text{ mol m}^{-2}\text{year}^{-1}$ ) off the Rio de la Plata mouth, with hardly any depth-dependence (cf. Hensen et al. 2000). Offshore, the Argentine Basin has been found to be a sink for biogenic opal and organic carbon (Hensen et al. 1998, 2000; Seiter et al. 2004) and a source of silica. Thus, silica fluxes  $J_{Si \text{ grid}}$  reach  $0.2 \text{ mol m}^{-2}\text{year}^{-1}$ .

### Statistically evaluated flux estimations

Verification of the reliability of the silica flux distribution pattern is based on a comparison between modelled and exponentially fitted  $J_{Si}$  data, by means of linear regression analysis. The dataset, recalculated after Holstein and Hensen (2010; cf. Table 2, Fig. 4a), shows a highly significant relationship between  $J_{Si \text{ mod.}}$  and  $J_{Si \text{ exp.}}$  ( $r^2 = 0.896$ ,  $SD = 0.078$ , t-test,  $p < 0.0001$ ,  $n = 24$ ).

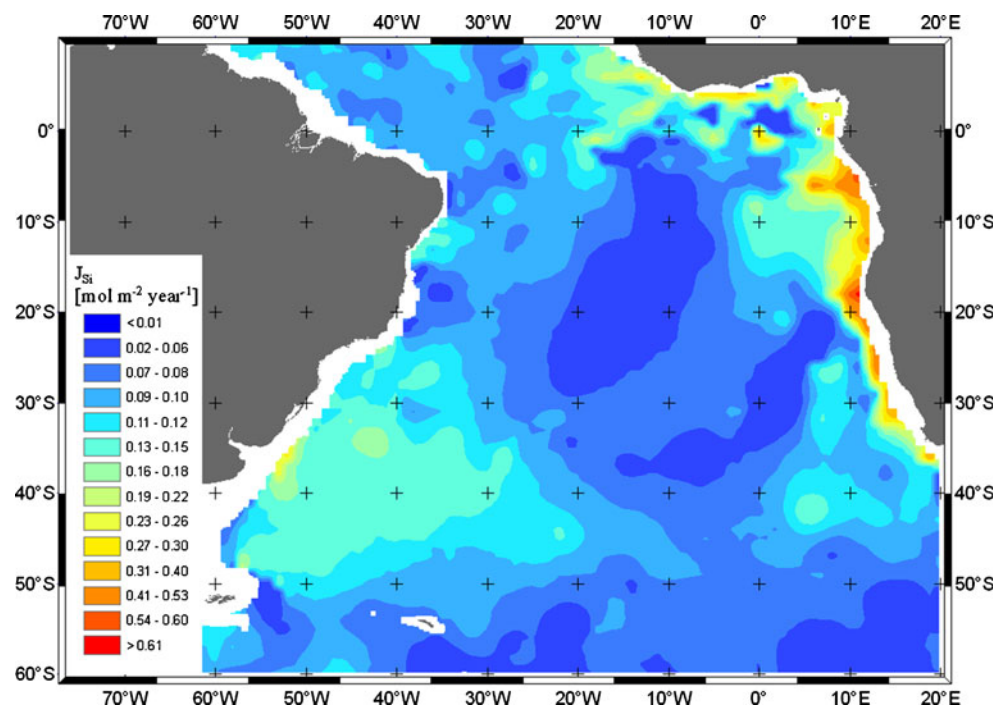
**Fig. 2** Basin-wide distribution of diffusive benthic oxygen uptake,  $J_{O_2 \text{ grid}}$ , extracted from Seiter et al. (2005) and excluding water depths <1,000 m



According to Holstein and Hensen (2010), the relationship between the modelled and exponentially fitted oxygen data ( $J_{O_2 \text{ mod.}}$  and  $J_{O_2 \text{ exp.}}$ ) is also very good ( $r^2=0.932$ ,  $SD=0.124$ , t-test,  $p<0.0001$ ,  $n=24$ ; cf. Table 2). Thus, the application of the coupling coefficient  $R_{Si/O_2}=0.52$  to the regular basin-wide grid of diffusive benthic oxygen fluxes  $J_{O_2 \text{ grid}}$  extracted from Seiter et al. (2005) should be a

promising tool for estimating further biogenic particle fluxes. According to Holstein and Hensen (2010), the exponential fits of Si profiles were mostly good but less accurate than the modelled fits, whereas modelled and exponential fits of oxygen fluxes were very similar. Nevertheless, gridded silica fluxes ( $J_{Si \text{ grid}}$ ) are significantly correlated with the modelled silica fluxes ( $J_{Si \text{ mod.}}$ ), with a

**Fig. 3** Basin-wide distribution of diffusive silica flux rates,  $J_{Si \text{ grid}}$ , calculated in the present study by applying  $R_{Si/O_2}$  to the  $J_{O_2 \text{ grid}}$  data (excluding water depths <1,000 m)





coefficient of determination  $r^2=0.636$  and a standard deviation of 0.104 (t-test,  $p<0.0001$ ,  $n=24$ , Fig. 4b, dashed line; modelled  $J_{Si}$  data extracted from Holstein and Hensen 2010, Table 2). The linear regression of the exponentially fitted data extracted from Holstein and Hensen (2010) has  $r^2=0.620$  and  $SD=0.101$  (t-test,  $p<0.0001$ ,  $n=24$ , not shown). Testing of the quality of the processed silica flux distribution pattern is based on the linear regression of all exponentially refitted data shown in Fig. 4b (solid line; cf. Tables 2 and 3, this study).  $J_{Si \text{ exp.}}$  vs.  $J_{Si \text{ grid}}$  data have  $r^2=0.514$  ( $SD=0.15$ , t-test,  $p<0.0001$ ,  $n=48$ ; solid line, Fig. 4b). It has to be

emphasized that, although the dataset of Table 3 was included neither into the calculations after Holstein and Hensen (2010) nor into the calculation of the silica flux distribution pattern, the predicted  $J_{Si \text{ grid}}$  values are reasonably correlated with previous estimates (Hensen et al. 1998).

On average, predicted silica grid values agree well with both the modelled and exponentially fitted data (Table 2). The quality of transformation of modelled or exponentially fitted data into gridded data can be expressed by the ratio of gridded silica fluxes and modelled or exponentially fitted data, with a ratio of 1 for the best fit. Gridded to modelled fluxes range from 0.33 to 1.86 for  $J_{Si \text{ grid}}: J_{Si \text{ mod.}}$  and from 0.41 to 1.63 for  $J_{Si \text{ grid}}: J_{Si \text{ exp.}}$ .

Regional fluctuations in the fitted data shown in Fig. 4b are particularly strong for the sedimentary provinces of the Cape Basin and the Argentine Basin, as has been previously documented in many studies (e.g. Hensen et al. 1998, 2000; Zabel et al. 1998). Especially the fitted data offshore the Namibian coastline south of 27°N of the Benguela upwelling cells, and in the southern part of the Argentine Basin show the most striking differences from the general trend (Fig. 4b, solid line and dotted line). The ratio of gridded silica fluxes vs. modelled silica fluxes ( $J_{Si \text{ grid}}: J_{Si \text{ mod.}}$ ) is very low for the southern Argentine Basin ( $J_{Si \text{ grid}}: J_{Si \text{ mod.}}=0.35$ ) and for the southern Cape Basin ( $J_{Si \text{ grid}}: J_{Si \text{ mod.}}=0.69$ ; Table 3), which means an underestimation of silica fluxes in this area by the mean  $R_{Si/O_2}=0.52$  calculated by Holstein and Hensen (2010). The best fit can be found for the northern Argentine Basin and the Angola and Guinea Basin with a mean  $J_{Si \text{ grid}}: J_{Si \text{ mod.}}$  ratio close to 1.

The validation of the transformation from point to gridded data by the exponentially refitted data, which was not included in the calculations after Holstein and Hensen (2010), can be shown by the ratio of gridded silica fluxes to exponentially refitted fluxes (Table 3, data from this study,  $J_{Si \text{ grid}}: J_{Si \text{ exp.}}$ ). Generally, the ratios range from 1.45 (min. 0.67, max. 2.58;  $SD=0.63$ ) for the Cape Basin to 1.55 (min. 0.46, max. 2.17,  $SD=0.57$ ) for the Angola and Guinea Basin. The mean ratios indicate overestimation of gridded silica fluxes in this area by the mean coupling coefficient  $R_{Si/O_2}=0.52$  calculated by Holstein and Hensen (2010). The general fluctuation of the calculated ratio  $J_{Si \text{ grid}}: J_{Si \text{ exp.}}$  is high, and regional patterns are not as noticeable as designated for the validation with data extracted from Holstein and Hensen (2010). Nevertheless, the results are in the same order of magnitude as for  $J_{Si \text{ grid}}: J_{Si \text{ mod.}}$ , with a general overestimation of  $J_{Si \text{ mod.}}$  of 50% and a range from -25 to 150%.

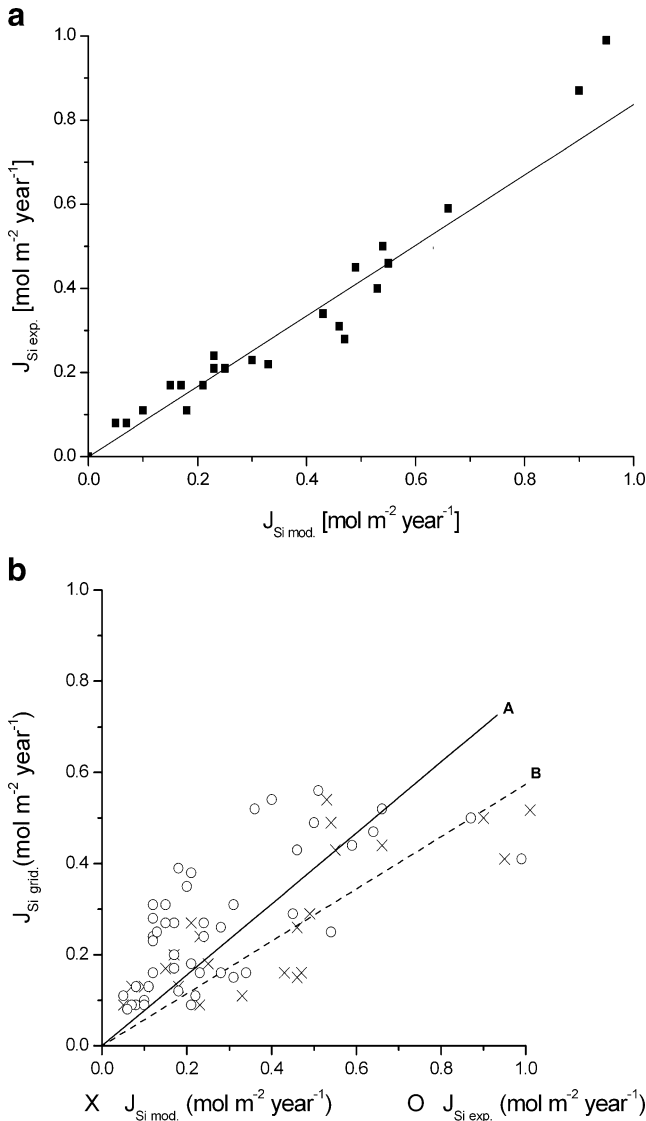


**Fig. 4** **a** Linear regression analysis of exponentially fitted and modelled silica flux rates (data extracted from Holstein and Hensen 2010,  $r^2=0.896$ ,  $SD=0.078$ ,  $n=24$ ). Data from water depths <1,000 m were excluded. **b** Comparison of estimated benthic silica fluxes derived from linear regression analyses of silica grid fluxes and either modelled silica fluxes or all exponentially fitted fluxes. *Solid line A*  $J_{Si \text{ grid}}$  vs.  $J_{Si \text{ exp.}}$ ,  $r^2=0.514$ ,  $n=48$ ; *dashed line B*  $J_{Si \text{ grid}}$  vs.  $J_{Si \text{ mod.}}$ ,  $r^2=0.636$ ,  $n=24$

### Quantification of benthic silica flux rates

Budgets of  $J_{Si \text{ grid}}$  were calculated for each benthic province (Table 4). In total, we estimated a benthic silica flux rate of

about 3.9 Tmol Si year<sup>-1</sup> for the investigated area of  $3.7 \times 10^{13} \text{ m}^2$  (cf. Figs. 1a and 3).

Lower rates are characteristic of basin areas whereas the highest silica fluxes were detected along the continental margins. The general  $J_{\text{Si grid}}$  flux budget in the deep-sea basin constitutes ~70% of the total flux, which is consistent with this basin representing 80% of the total study area. By contrast, the SWACO province accounts for roughly 11% of the total flux in only 5% of the total area (Fig. 5). Similarly, relatively high  $J_{\text{Si grid}}$  fluxes were recorded offshore the Congo River, so that 5% of the total flux (cf. 0.2 Tmol Si year<sup>-1</sup>) is remobilized from a relatively small area. These continental margin provinces can be regarded as most important for the total budget of the study area.

#### Regional distributions of biogenic particle fluxes

The highest biogenic particle rain rates predicted from the mineralized fraction were observed along the West African continental margin, especially offshore Namibia north of 30°S. By contrast, rain rates for the open ocean are expected to be low, with slightly increased values on the Santos Plateau offshore Brazil (Fig. 6a).

Calculation of the total flux  $J_{\text{P tot. grid}}$ , which includes the buried, refractory, and non-mineralizable or quickly settled fraction ( $\beta$ ), revealed a more complex pattern (Fig. 6b), which is in close relation to the bathymetry of the study area. For example, the Walvis Ridge, the Mid-Atlantic Ridge and the Santos Plateau are associated with higher particle rain rates than that of the adjacent deep-sea basin. The deep basin calculations show mean  $J_{\text{P tot. grid}}$  values ranging from 5 to 10  $\text{gm}^{-2}\text{year}^{-1}$ , whereas total fluxes are approx. 20  $\text{gm}^{-2}\text{year}^{-1}$  on average on the Mid-Atlantic Ridge and ~40  $\text{gm}^{-2}\text{year}^{-1}$  on the Santos Plateau.

The mineralizable fraction of biogenic particles ( $J_{\text{P min. grid}}$ ) was found to be high off the coast of Namibia (max. 135  $\text{gm}^{-2}\text{year}^{-1}$ ), with occasionally slightly increased total biogenic fluxes. Similar fluxes were calculated in the Congo catchment area, albeit displaying minor differences between  $J_{\text{P min. grid}}$  and  $J_{\text{P tot. grid}}$  (Table 5).

The main constituent of biogenically formed particles settling to the seafloor is calcite, particularly offshore Namibia and the Congo River mouth where it constitutes up to 66 and 62% of total biogenic fluxes respectively. In these regions, corresponding values of opal accumulation are only 27 and 30% respectively. Six percent of the area-dependent total calcite rain rate is buried ( $\beta$ ) offshore Namibia, but only 3% offshore the Congo River where an increased total opal burial rate of 4% prevails. Here, calculated calcite preservation is of little importance (cf. only 0.5%, calculated by using measured and modelled data, Eqs. 5 and 6, Table 5).

Consistent with the error of transformation of  $J_{\text{Si mod.}}$  to  $J_{\text{Si grid}}$  (cf. above), there is a maximum error range of 2 between the grid calculations of particle rain rates and those calculated from modelled fluxes (Table 5).

#### Discussion and conclusions

The application of oxygen fluxes as a proxy parameter in this study is a new and essentially simple approach to calculate reliable silica budgets and evaluate biogenic flux particles, in particular of opal. Our approach is based on the interrelation between the decay of organic carbon on organic surfaces catalysed by microbes and the associated increase of the opal mineral surface area observed in the water column (Bidle et al. 2003). Hence, as demonstrated by Bidle et al. (2003), the dissolution of sedimentary biogenic opal is accelerated, accompanied by increasing benthic silica fluxes. Following this approach, we inferred a correlation between sedimentary opal and total organic carbon, and calculated silica fluxes by relating benthic diffusive oxygen fluxes to silica flux rates according to the equation of Holstein and Hensen (2010). Biogenic opal particle fluxes were deduced accordingly. Furthermore, we compiled published relations of calcite dissolution to aerobic organic carbon mineralization, and assessed particle fluxes of calcite and organic carbon (Pfeifer et al. 2002; Seiter et al. 2005).

#### Comparison of regional and global silica budgets

The calculated budgets determined in our study area agree very well with previous investigations. Tréguer et al. (1995) and Tréguer (2002) reported a mean PP of 240 Tmol Si year<sup>-1</sup> for the global ocean, an area of  $\sim 3.7 \times 10^{13} \text{ m}^2$ . In our study area, we calculated primary production of approx. 25 Tmol Si year<sup>-1</sup>, along with a calculated benthic rain rate of the mineralizable fraction of biogenic opal ( $J_{\text{Si grid}}$ ) of 3.9 Tmol Si year<sup>-1</sup>. This is equivalent to 16% of the particle rain being related to primary opal production. Tréguer et al. (1995) and Tréguer (2002) calculated 12%, and Nelson et al. (1995) reported a range of 15–25%. The estimations of Ridgwell et al. (2002), yielding a value 35% relative to primary-produced silica, constitute the upper boundary of global calculations. The calculation derived from the present study considers both the mineralizable fraction of biogenic particles and the total flux, including the buried fraction. The buried fraction in the study area was calculated to be 0.32 Tmol Si year<sup>-1</sup>, whereas Tréguer et al. (1995) and Tréguer (2002) estimated a value of 0.6 Tmol Si year<sup>-1</sup> for the same area. Since global estimates do not necessarily correspond to the budgets derived from the South Atlantic, the present comparison should be regarded

**Table 4** Total budgets of diffusive benthic silica fluxes in specific provinces, and minimum, maximum, mean and standard deviation (SD) values for the processed grid ( $J_{Si\ grid}$ )

Provinces	Surface area <sup>a</sup> (m <sup>2</sup> )	Min. $J_{Si\ grid}$ (mol m <sup>-2</sup> year <sup>-1</sup> )	Max. $J_{Si\ grid}$	Mean $J_{Si\ grid}$	SD	Total budget (Tmol year <sup>-1</sup> )
SWACO <sup>b</sup>	1.8E+12	0.07	0.62	0.25	0.11	0.45
GUI	1.8E+11	0.04	0.31	0.22	0.07	0.04
GUBRACO	6.6E+11	0.06	0.14	0.10	0.01	0.06
SOATL	2.7E+13	0.03	0.26	0.09	0.03	2.76
NOATL	3.2E+11	0.03	0.20	0.10	0.02	0.31
ARGCO	4.1E+11	0.05	0.19	0.09	0.03	0.04
BRAZCO	9.2E+11	0.04	0.17	0.11	0.03	0.096
RIOPLATA	4.1E+11	0.06	0.28	0.15	0.04	0.05
NAMBCO	3.4E+11	0.07	0.62	0.30	0.14	0.10
ETROPAT <sup>c</sup>	4.0E+12	–	–	–	–	0.59
ETROPAT* <sup>d</sup>	2.0E+12	0.01	0.60	0.15	0.08	0.35
CONGO	8.7E+11	0.07	0.60	0.23	0.10	0.20
Total	3.7E+13					3.9

<sup>a</sup> Excluding water depth <1,000 m

<sup>b</sup> Including NAMBCO and CONGO plume region

<sup>c</sup> Equatorial Atlantic (ETROPAT) calculated including continental margin off Guinea (GUI) and the CONGO freshwater plume region

<sup>d</sup> Equatorial Atlantic (ETROPAT\*) calculated excluding the CONGO plume region

as a rough approximation, indicating that our estimation is within a reasonable order of magnitude of former findings.

van Bennekom and Berger (1984) detected a regional riverine discharge of 0.23 Tmol Si year<sup>-1</sup> dissolved silica in the Congo River, which is consistent with the regional budget we calculated for this area. Still, our estimate exceeds the budget calculated for the study area by Hensen et al. (1998) by a factor of 1.6, which is most likely related to regionally strongly variable factors like lateral inputs, which cannot be resolved in detail by the applied general correlation between oxygen and silica fluxes.

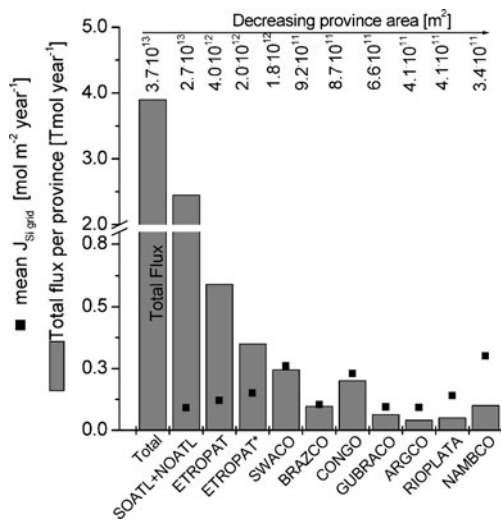


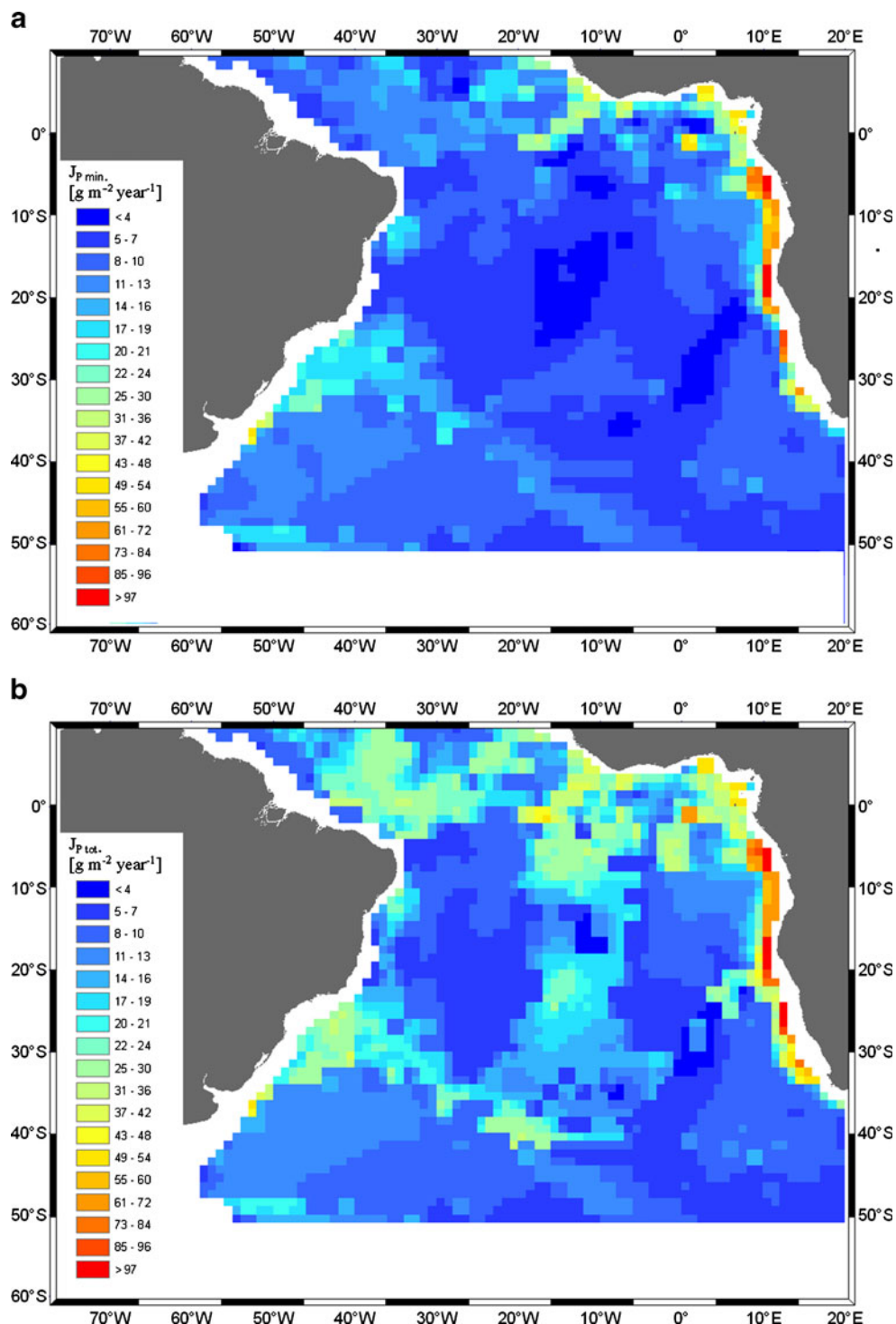
**Fig. 5** Budgeting of total silica fluxes in specific provinces (according to Seiter et al. 2004; shaded columns, Tmol year<sup>-1</sup>). Closed squares Mean  $J_{Si\ grid}$  in each province (mol m<sup>-2</sup> year<sup>-1</sup>), ETROPAT\* equatorial Atlantic budget, excluding the offshore freshwater Congo River fan region (see text for explanation of other province names)

Reliability of silica flux calculations and estimation error

In the present study, one criterion of quality is the coefficient of determination,  $r^2$ , of the regression analysis. The scatter of  $J_{Si\ grid}$  values obtained from modelled or exponentially calculated data can be expressed by  $r^2=0.636$  for modelled data versus grid data (dashed line B in Fig. 4b) and  $r^2=0.514$  for exponentially fitted data (solid line A in Fig. 4b). On the one hand, the quality of estimation of modelled fluxes is better than the exponentially refitted fluxes as reported by Holstein and Hensen (2010) but, on the other hand, the quality of the main matrix, i.e.  $J_{O_2\ grid}$  (cf. Seiter et al. 2005), is crucial and should not be neglected.  $J_{O_2\ grid}$  was originally processed by applying a total organic carbon grid (Seiter et al. 2004). Consequently, the estimation error of 2 recorded for the TOC grid is transmitted to both later estimates,  $J_{O_2\ grid}$  and  $J_{Si\ grid}$ .

Generally, variations in Si:O<sub>2</sub> flux ratios would be of minor importance for the basin-wide area if we hypothesize a coupling of Si:O<sub>2</sub> in the sediment similar to that published by Ragueneau et al. (2000) with regard to particulate Si:C ratios in the water column at latitudes between 10°N and 50°S. However, some problems arise by using a single, mean  $R_{Si/O_2}$  ratio for all continental margins, because the regional differences in  $R_{Si/O_2}$  values recorded at the individual study sites become suppressed. Grid values were indeed underestimated in the southern Cape Basin (sites GeoB 3702, GeoB 3703, Table 2), offshore Namibia and in the Walvis Ridge region by applying a mean ratio ~35% lower than the regional ratio (site GeoB 3702). Especially offshore Namibia, intense primary productivity promotes the preservation of organic matter, associated with stagnant  $J_{O_2}$  and higher TOC contents (Wenzhoefer and Glud 2002; Seiter et al. 2005). Thus, applying the mean  $R_{Si/O_2}=0.52$

**Fig. 6** **a** Basin-wide distribution of minimum biogenic particle fluxes to the seafloor,  $J_{P \text{ min. grid}}$  ( $\text{g m}^{-2} \text{ year}^{-1}$ ). **b** Basin-wide distribution of total biogenic particle fluxes to the seafloor,  $J_{P \text{ tot. grid}}$  ( $\text{g m}^{-2} \text{ year}^{-1}$ )



calculated by Holstein and Hensen (2010), instead of the regional  $R_{\text{Si}/\text{O}_2}$  value of 0.63, results in a regional underestimation of  $J_{\text{Si grid}}$ . The results from the Argentine Basin show a regional  $R_{\text{Si}/\text{O}_2}=0.44$  and thus should result in an overestimation of  $J_{\text{Si grid}}$  values, which is not evident from our findings except for the northern Argentine Basin, where a slight overestimation is predicted. The north-eastern Angola

Basin is strongly influenced by discharge of the Congo River. Relatively low  $R_{\text{Si}/\text{O}_2}$  ratios in this region (0.31 to 0.56) could therefore be explained by the high riverine input of aluminium, which reduces the solubility of biogenic silica (e.g. van der Gaast and Jansen 1984; van Bennekom et al. 1989; van Cappellen and Qiu 1997; Dixit et al. 2001; Dixit and van Cappellen 2002; Gallinari et al. 2002).

**Table 5** Major biogenic components of surface sediments, burial rates ( $\beta$ ) and calculated biogenic particle fluxes to the seafloor (this study;  $J_{p \text{ min}}$  = minimum particle flux,  $J_{p \text{ tot}}$  = total particle flux) at continental margin sites ( $n=24$ ) in the Southern Atlantic Ocean (*n.v.* not validated)

Core no.	TOC (dry wt%)	Opal	Calcite	SR <sup>a</sup> (cm 1,000year <sup>-1</sup> )	DBD <sup>b</sup> (g cm <sup>-3</sup> )	$\beta_{\text{calculated}}^c$ (g m <sup>-2</sup> year <sup>-1</sup> )	$\beta_{\text{calcite}}^c$	$\beta_{\text{opale}}^c$	$J_p$ min. <sup>d</sup> grid	$J_p$ min. <sup>e</sup> mod.	$J_{p \text{ tot.}}^d$ grid	$J_{p \text{ tot.}}^e$ mod.	$J_{p \text{ tot.}}^c$ calcite	$J_{p \text{ tot.}}^e$ opal	$J_{p \text{ tot.}}^e$ mod.	$\Delta\text{CO}_3$ <0	Reference <sup>g</sup>	
																	TOC	Opal
GeoB 4906	1.51	2.51	4.90	4.20	0.35	1.31	1.22	0.72	0.37	42.9	94.2	44.2	95.4	60.1	26.7	3	1	7
GeoB 4909	1.32	1.35	12.3	4.20	0.41	2.58	0.80	2.12	0.23	33.1	55.1	33.9	57.8	35.2	16.5	3	1	7
GeoB 4913	1.65	4.31	0.10	12.1	0.36	2.64	0.68	0.04	1.88	116.0	112	116.7	115	71.3	32.7	8	1	6
GeoB 4917	2.16	1.54	0.30	8.10	0.41	1.33	2.59	0.10	0.51	82.4	116	82.8	117	73.9	32.3	8	1	6
GeoB 4901	0.80	4.46	4.50	6.90	0.38	2.56	1.18	1.18	1.17	55.4	23.5	56.6	25	19.8	11.9	3	1	7
GeoB 3702	3.10	1.01	52.4	9.90	0.23	12.9	14.6	11.9	0.23	87.8	162	102.4	175	117.1	44.0	3	5	6
GeoB 3703	6.10	1.80	45.8	14.5	0.22	17.1	10.0	14.6	0.57	101.5	225	111.5	243	122.3	45.3	3	5	6
GeoB 3705	4.00	2.08	51.0	2.90	0.19	3.15	11.3	2.81	0.11	101.1	80	101.3	91.1	51.1	22.2	3	5	6
GeoB 3706	4.53	0.85	58.9	3.10	0.2	3.99	14.5	3.65	0.05	92.9	185	107.4	195	99.5	40.3	3	5	6
GeoB 3707	3.74	0.48	55.6	3.70	0.12	2.66	15.1	2.47	0.02	58.1	141	73.2	147	94.0	38.6	3	1	6
GeoB 3715	4.92	1.90	45.3	3.60	0.19	3.57	9.67	3.10	0.13	103.8	102	103.9	109	64.1	27.1	3	1	6
GeoB 3719	3.10	n.v.	25.6	9.10	0.24	n.v.	5.22	5.59	n.v.	112.7	133	117.9	140	n.v.	n.v.	3	-	4
GeoB 6202	2.74	n.v.	62.0	7.90	0.25	n.v.	13.1	12.25	n.v.	77.0	48.8	90.1	65	n.v.	n.v.	3	5	6
GeoB 6214	0.96	0.57	1.00	0.50	0.29	0.04	1.15	0.01	0.01	20.5	18.5	21.7	18.9	10.2	7.5	3	1	4
GeoB 6219	2.48	2.34	n.v.	4.21	0.35	n.v.	0.17	n.v.	0.34	n.v.	41.2	n.v.	47.6	n.v.	n.v.	3	1	-
GeoB 6223	1.19	6.26	n.v.	3.69	0.18	n.v.	0.10	n.v.	0.42	29.8	27.3	29.9	28.4	n.v.	n.v.	3	4	-
GeoB 6226	0.50	n.v.	0.00	5.00	0.49	n.v.	0.23	n.v.	n.v.	11.6	16.9	11.8	16.9	n.v.	n.v.	3	4	9
GeoB 6229	1.07	n.v.	n.v.	11.6	0.58	n.v.	0.79	n.v.	n.v.	10.2	8.6	11.0	8.6	n.v.	n.v.	3	4	-
GeoB 6230	1.49	4.00	0.70	8.30	0.47	2.41	0.66	0.27	1.56	46.7	53.8	47.4	57.1	30.8	16.8	3	4	9
GeoB 6230	1.02	n.v.	n.v.	4.30	0.29	n.v.	1.02	n.v.	n.v.	13.5	33.7	16.7	33.7	n.v.	n.v.	3	4	-
GeoB 6230	0.77	n.v.	11.7	8.40	0.37	n.v.	0.84	3.64	n.v.	16.7	43.6	17.6	43.6	n.v.	n.v.	3	4	6

Table 5 (continued)

Core no.	TOC	Opal	Calcite	SR <sup>a</sup> (cm 1,000year <sup>-1</sup> )	DBD <sup>b</sup> (g cm <sup>-3</sup> )	$\beta_{\text{calculated}}^c$ (g m <sup>-2</sup> year <sup>-1</sup> )	$\beta_{\text{grind}}^c$	$\beta_{\text{grind}}^c$ calcite <sup>e</sup>	$\beta_{\text{grind}}^c$ opal <sup>e</sup>	$J_P$ min. grid <sup>d</sup>	$J_P$ min. mod. <sup>e</sup>	$J_P$ <sup>tot.</sup> grid <sup>d</sup>	$J_P$ <sup>tot.</sup> mod. <sup>e</sup>	$J_P$ <sup>tot.</sup> calcite <sup>e</sup> mod. <sup>e</sup>	$J_P$ <sup>tot.</sup> opal <sup>e</sup> mod. <sup>e</sup>	$\Delta\text{CO}_3$ f <0	Reference <sup>g</sup>		
																	TOC	Opal	Calcite
2704	1.33	n.v.	1.80	8.70	0.25	n.v.	0.95	0.39	n.v.	12.1	36.2	13.1	36.2	n.v.	n.v.	<0	3	4	6
2705	0.50	n.v.	0.30	8.00	0.51	n.v.	1.57	0.12	n.v.	8.7	30.4	10.3	30.4	n.v.	n.v.	<0	3	4	6
2706	0.40	n.v.	13.3	11.6	0.16	n.v.	1.17	2.47	n.v.	11.9	89.2	13.1	92.1	n.v.	n.v.	<0	3	4	6
2707	0.64	n.v.	n.v.	9.20	0.13	n.v.	n.v.	0.07	n.v.	6.6	n.v.	n.v.	19	n.v.	n.v.	<0	2	–	2
4417																			

<sup>a</sup> SR, data based on sedimentation rate grid after Mollenhauer et al. (2004)

<sup>b</sup> DBD, data based on dry bulk density grid after Mollenhauer et al. (2004)

<sup>c</sup>  $\beta$ , estimated burial rate of biogenic particles (see Eq. 6);  $\beta_{\text{calculated}}$  based on data in Table 5;  $\beta_{\text{grind}}$  based on grid data after Mollenhauer et al. (2004)

<sup>d</sup>  $J_P$  min. grid and  $J_P$  tot. grids, minimum and total particle fluxes respectively, based on calculated oxygen flux grid data after Seiter et al. (2005)

<sup>e</sup>  $J_P$  min. mod. and  $J_P$  tot. mod., minimum and total particle fluxes respectively, calculated using modelled oxygen fluxes after Holstein and Hensen (2010)

<sup>f</sup> Calcite saturation state of water column after Archer (1996)

<sup>g</sup> References: 1, Holstein (2002); 2, Wenzhoefer (1999); 3, Mollenhauer et al. (2004); 4, Romero and Hensen (2002); 5, Schulz (2000); 6, Hensen et al. (1998); 7, Pfeifer et al. (2002); 8, Wagner et al. (2004); 9, Riedinger et al. (2005)

Overall, the hypothesis presented in this study is still based on very limited data. It should also be noted that although this new estimative approach to evaluate silica flux rates cannot exclude effects induced by seasonal variations, these are considered to be negligible at a basin-wide scale. Despite the uncertainties associated with this approach (cf. above), it is emphasized that the incorporation of appropriate control parameters, such as  $J_{O_2}$  and TOC, has the major advantage of providing a wealth of additional spatial information, especially with regard to data resolution.

Comparison with biogenic particle fluxes based on trap data: An example from trap station GBZ5 (south guinea basin)

The evaluation of biogenic particle fluxes (calcite, opal, organic carbon) based on the aerobic metabolization of organic carbon in the deep sea is particularly convenient if the limited size of the database derived from deep-sea particle traps is considered. Nevertheless, the approximation of real biogenic particle fluxes depends on some basic assumptions possibly associated with inaccuracies other than the statistical ones discussed above. Notably, calcite particle fluxes were calculated on the basis of calcite dissolution rates mediated by aerobic organic carbon mineralization above the hydrographical lysocline (cf. Pfeifer et al. 2002). If suboxic and anoxic diagenesis become more important than oxic diagenesis, then the applied relation may not hold true and potentially lead to an underestimation of calcite particle fluxes. This could apply to the high productivity region off Namibia. By contrast, the upper limit of the relationship is determined by calcite supply. Thus, if calcite is exhausted, for example, below the hydrographical lysocline, but aerobic organic carbon mineralization still occurs, then a strong overestimation of calcite particle rain will result. Overestimations below the lysocline were excluded in this study, as we deliberately did not extrapolate particle fluxes below the lysocline (Fig. 6a, b).

As an example of comparison between particle fluxes derived from deep-sea trap data and the estimation made in this study, data from trap station GBZ5 (water depth 3,920 m, trap depth 3,382 m; 9°52.0'W, 2°02.0'S; Lampitt and Antia 1997) can be used. This trap recorded a rate of 26.7 g  $CaCO_3$   $m^{-2}$   $year^{-1}$ , the biogenic calcite component here constituting ~76% of the total biogenic flux, in contrast to a value of 60% calculated in the present study. The relationship published by Pfeifer et al. (2002) was validated with data obtained northwards of the Congo River, which show only moderate turnover rates. The sediments at this location contain higher amounts of low-reactivity organic matter (Wagner et al. 2004), and

increased enrichment of opal was also reported by van der Gaast and Jansen (1984). However, for biogenic opal, an amount of 5.9 g  $SiO_2$   $m^{-2}$   $year^{-1}$  was recorded by the trap, compared to 4.6 g  $SiO_2$   $m^{-2}$   $year^{-1}$  derived in our estimation of  $J_{Si}$   $_{grid}$ . The two values differ by a factor of 1.3, which is essentially within the margin of error discussed above (cf. factor 2).

Nevertheless, there are considerable uncertainties with regard to particle flux values based on trap data. For example, strong bottom currents would cause advective transport of suspended particles in the water column or at the seafloor. The sinking velocity of opal or calcite is faster than that of organic carbon (Klaas and Archer 2002), and more energy would be required for the transport of such heavier components. This could be the reason why Seiter et al. (2005) calculated only half of the particulate organic carbon as being collected via vertical transport at this trap location (cf. Lampitt and Antia 1997; Fischer et al. 2000), the remainder being due rather to lateral transport.

Notwithstanding the considerable advantage of estimating particle fluxes in terms of proxy parameters such as aerobic organic carbon mineralization, it remains necessary to develop regionally dependent  $R_{Si/O_2}$  ratios in future investigations. This will require an extension of the current database of silica and oxygen flux data. In addition, more deep-sea trap data are needed to evaluate particle flux estimations, particularly in terms of lateral transport.

**Acknowledgements** We thank H. Hecht, K. Pfeifer and N. Riedinger for valuable discussions during the development of this work. This manuscript has benefited from critical review comments by R.W. Murray, C.L. Ziegler and M.T. Delafontaine. We thank the Deutsche Forschungsgemeinschaft for funding this research (DFG, ZA 199/1-1).

## References

- Aller RC, Aller JY (1998) The effect of biogenic irrigation intensity and solute exchange on diagenetic reaction rates in marine sediments. *J Mar Res* 56:905–936
- Antia AN, Koeve W, Fischer G, Blanz T, Schulz-Bull D, Scholten J, Neuer S, Kremling K, Kuss J, Peinert R, Hebbeln D, Bathmann U, Conte M, Fehner U, Zeitschel B (2001) Basin-wide particulate carbon flux in the Atlantic Ocean: regional export patterns and potential for atmospheric  $CO_2$  sequestration. *Glob Biogeochem Cycles* 15:845–862
- Antoine D, André J-M, Morel A (1996) Oceanic primary production—2: estimation at global scale from satellite (coastal zone color scanner) chlorophyll. *Glob Biogeochem Cycles* 10:57–69
- Archer DE (1996) An atlas of the distribution of calcium carbonate in sediments of the deep sea. *Glob Biogeochem Cycles* 10:159–174
- Behrenfeld MJ, Falkowski PG (1997) Photosynthetic rates derived from satellite-based chlorophyll concentration. *Limnol Oceanogr* 42(1):1–20
- Berelson WM, Balch WM, Najjar R, Feely RA, Sabine C, Lee K (2007) Relating estimates of  $CaCO_3$  production, export, and dissolution in the water column to measurements of  $CaCO$  rain

- into sediment traps and dissolution on the sea floor: a revised global carbonate budget. *Glob Biogeochem Cycles* 21:GB1024. doi:10.1029/2006GB002803
- Berger WH, Smetacek VS, Wefer G (1989) Ocean productivity and paleoproductivity—an overview. In: Berger WH, Smetacek VS, Wefer G (eds) *Productivity of the ocean: present and past*. Dahlem Workshop Reports. Wiley, Chichester, pp 1–34
- Bidle KD, Azam F (1999) Accelerated dissolution of diatom silica by marine bacterial assemblages. *Nature* 397:508–512
- Bidle KD, Brzezinski MA, Long RA, Jones JL, Azam F (2003) Diminished efficiency in the oceanic silica pump caused by bacteria-mediated silica dissolution. *Limnol Oceanogr* 48:1855–1868
- Brzezinski MA (1985) The Si:C:N ratio of marine diatoms: interspecific variability and the effect of some environmental variables. *J Phycol* 21:347–357
- Christensen JP (2000) A relationship between deep-sea benthic oxygen demand and oceanic primary productivity. *Oceanol Acta* 23:65–82
- DeMaster DJ (1981) The supply and accumulation of silica in the marine environment. *Geochim Cosmochim Acta* 45:1715–1732
- Dixit S, van Cappellen P (2002) Surface chemistry and reactivity of biogenic silica. *Geochim Cosmochim Acta* 66:2559–2568
- Dixit S, van Cappellen P, van Bennekom AJ (2001) Processes controlling solubility of biogenic silica and pore water build-up of silicic acid in marine sediments. *Mar Chem* 73:333–352
- Fischer G, Ratmeyer V, Wefer G (2000) Organic carbon fluxes in the Atlantic and the Southern Ocean: relationship to primary production compiled from satellite radiometer data. *Deep-Sea Res Part II* 47(9/11):1961–1997
- Froelich PN, Klinkhammer GP, Bender ML, Luedtke NA, Heath GR, Cullen D, Dauphin P, Hammond D, Hartman B, Maynard V (1979) Early oxidation of organic matter in pelagic sediments of the eastern equatorial Atlantic: suboxic diagenesis. *Geochim Cosmochim Acta* 43(7):1075–1090
- Gallinari M, Ragueneau O, Corrin L, DeMaster DJ, Tréguer P (2002) The importance of water column processes on the dissolution properties of biogenic silica in deep-sea sediments. I. Solubility. *Geochim Cosmochim Acta* 66:2701–2717
- Ganachaud A, Wunsch C (2002) Oceanic nutrient and oxygen transports and bounds on export production during the World Ocean Circulation Experiment. *Glob Biogeochem Cycles* 16(4):1057. doi:10.1029/2000GB001333
- Glud RN, Gundersen JK, Revsbech NP, Jørgensen BB (1994) Effects on the benthic diffusive boundary layer imposed by micro-electrodes. *Limnol Oceanogr* 39:462–467
- Gundersen JK, Jørgensen BB (1990) Microstructure of diffusive boundary layer and the oxygen uptake of the seafloor. *Nature* 345:604–607
- Hensen C, Landenberger H, Zabel M, Schulz HD (1998) Quantification of diffusive benthic fluxes of nitrate, phosphate and silicate in the Southern Atlantic Ocean. *Glob Biogeochem Cycles* 12:193–210
- Hensen C, Zabel M, Schulz HD (2000) A comparison of benthic nutrient fluxes from deep-sea sediments off Namibia and Argentina. *Deep-Sea Res Part II* 47(9/11):2029–2050
- Holstein JM (2002) Effekt benthischer Mineralisationsprozesse auf die Lösung von biogenem Opal. Diploma Thesis, Department of Geosciences, University of Bremen, Germany
- Holstein JM, Hensen C (2010) Microbial mediation of benthic biogenic silica dissolution. *Geo-Mar Lett* 30, in press. doi:10.1007/s00367-009-0181-3
- Honjo S, Manganini SJ, Krishfield RA, Francois R (2008) Particulate organic carbon fluxes to the ocean interior and factors controlling the biological pump: a synthesis of global sediment trap programs since 1983. *Prog Oceanogr* 76:217–285
- Jahnke RA (1996) The global ocean flux of particulate organic carbon: areal distribution and magnitude. *Glob Biogeochem Cycles* 10:71–88
- Kemp AES, Pearce RB, Grigorov I, Lange CB, Quilty P, Salter I (2006) Production of giant marine diatoms and their export at oceanic frontal zones: implications for Si and C flux from stratified oceans. *Glob Biogeochem Cycles* 20:GB4S04. doi:10.1029/2006GB002698
- Klaas C, Archer DE (2002) Association of sinking organic matter with various types of mineral ballast in the deep sea: implications for the rain ratio. *Glob Biogeochem Cycles* 16(4):1116. doi:10.1029/2001GB001765
- Lampitt RS, Antia AN (1997) Particle flux in the deep seas: regional characteristics and temporal variability. *Deep-Sea Res I* 44:1377–1403
- Lampitt RS, Salter I, Johns D (2009) Radiolaria: major exporters of organic carbon to the deep ocean. *Glob Biogeochem Cycles* 23:GB1010. doi:10.1029/2008GB003221
- Mollenhauer G, Schneider RR, Müller PJ, Spieß V, Wefer G (2002) Glacial/interglacial variability in the Benguela upwelling system: spatial distribution and budgets of organic carbon accumulation. *Glob Biogeochem Cycles* 16:1134. doi:10.1029/2001GB001488
- Mollenhauer G, Schneider RR, Jennerjahn TC, Müller PJ, Wefer G (2004) Organic carbon accumulation in the South Atlantic Ocean: its modern, mid-Holocene and last glacial basin-wide distribution. *Glob Planet Change* 40(3/4):249–266
- Moriceau B, Gallinari M, Soetaert K, Ragueneau O (2007a) Importance of particle formation to reconstructed water column biogenic silica fluxes. *Glob Biogeochem Cycles* 21:GB3012. doi:10.1029/2006GB002814
- Moriceau B, Garvey M, Ragueneau O, Passow U (2007b) Evidence for reduced biogenic silica dissolution rates in diatom aggregates. *Mar Ecol Prog Ser* 333:129–142
- Nelson DM, Tréguer P, Brzezinski MA, Leynaert A, Queguiner B (1995) Production and dissolution of biogenic silica in the ocean: revised global estimates, comparison with regional data and relationship to biogenic sedimentation. *Glob Biogeochem Cycles* 9:359–372
- Pfeifer K, Hensen C, Adler M, Wenzhoefer F, Weber B, Schulz HD (2002) Modeling of subsurface calcite dissolution including the respiration and reoxidation processes of marine sediments in the region of equatorial upwelling off Gabon. *Geochim Cosmochim Acta* 66(24):4247–4259
- Rabouille C, Gaillard J-F, Tréguer P, Vincendeau M-A (1997) Biogenic silica recycling in surficial sediments across the polar front of the Southern Ocean (Indian Sector). *Deep-Sea Res II* 44(5):1151–1176
- Ragueneau O, Tréguer P, Leynaert A, Anderson RF, Brzezinski MA, DeMaster DJ, Dugdale RC, Dymond J, Fischer G, Francois R, Heinze C, Maier-Reimer E, Martin-Jézéquel V, Nelson DM, Quéguiner B (2000) A review of the Si cycle in the modern ocean: recent progress and missing gaps in the application of biogenic opal as a paleoproductivity proxy. *Glob Planet Change* 26:317–365
- Ragueneau O, Schultes S, Bidle K, Claquin P, Moriceau B (2006) Si and C interactions in the world ocean: importance of ecological processes and implications for the role of diatoms in the biological pump. *Glob Biogeochem Cycles* 20:GB4S02. doi:10.1029/2006GB002688
- Redfield AC (1958) The biological control of chemical factors in the environment. *Am Sci* 9:205–221
- Ridgwell AJ, Watson AJ, Archer DE (2002) Modeling the response of the oceanic Si inventory to perturbation, and consequences for atmospheric CO<sub>2</sub>. *Glob Biogeochem Cycles* 16(4):1071. doi:10.1029/2002GB001877



- Riedinger N, Pfeifer K, Kasten S, Garming JFL, Vogt C, Hensen C (2005) Diagenetic alteration of magnetic signals by anaerobic oxidation of methane related to a change in sedimentation rate. *Geochim Cosmochim Acta* 69:4117–4126
- Romero O, Hensen C (2002) Oceanographic control of biogenic opal and diatoms in surface sediments of the Southwestern Atlantic. *Mar Geol* 186:263–280
- Sayles FL, Deuser WG, Goudreau JE, Dickinson WH, Jickells TD, King P (1996) The benthic cycle of biogenic opal at the Bermuda Atlantic Time Series site. *Deep-Sea Res I* 43(4):383–409
- Schlitzer R (2002) Carbon export fluxes in the Southern Ocean: results from inverse modeling and comparison with satellite-based estimates. *Deep-Sea Res II* 49(9/10):1623–1644
- Schulz S (2000) Frühdiagenese von Opal in Oberflächensedimenten des Süd-Atlantiks. Versuch einer Bilanzierung. Diploma Thesis, Department of Geosciences, University of Bremen, Germany
- Seiter K, Hensen C, Schröter J, Zabel M (2004) Organic carbon content in surface sediments—defining regional provinces. *Deep-Sea Res I* 51(12):2001–2026
- Seiter K, Hensen C, Zabel M (2005) Benthic carbon mineralization on a global scale. *Glob Biogeochem Cycles* 19:GB1010. doi:10.1029/2004GB002225
- Shannon LV, Nelson G (1996) The Benguela: large scale features and processes and system variability. In: Wefer G, Berger WH, Siedler G (eds) *The South Atlantic: present and past circulation*. Springer, Berlin, pp 163–210
- Thomsen L (2003) The benthic boundary layer. In: Wefer G, Billett D, Hebbeln D, Jørgensen BB, Schlüter M, van Weering TCE (eds) *Ocean margin systems*. Springer, Berlin, pp 143–155
- Tréguer P (2002) Silica and the cycle of carbon in the ocean. *Geoscience* 334:3–11
- Tréguer P, Nelson DM, van Bennekom AJ, DeMaster DJ, Leynaert A, Queguiner B (1995) The balance of silica in the world ocean: a re-estimate. *Science* 268:375–379
- van Andel TH (1975) Mesozoic/Cenozoic calcite compensation depth and global distribution of calcareous sediments. *Earth Planet Sci Lett* 26:187–194
- van Bennekom AJ, Berger GW (1984) Hydrography and silica budget of the Angola basin. *Neth J Sea Res* 17:149–200
- van Bennekom AJ, Jansen JHF, van der Gaast SJ, van Iperen JM, Pieters J (1989) Aluminium-rich opal: an intermediate in the preservation of biogenic silica in the Zaire (Congo) deep-sea fan. *Deep-Sea Res A* 36(2):173–190
- van Cappellen P, Qiu L (1997) Biogenic silica dissolution in sediments of the Southern Ocean. I. Solubility. *Deep-Sea Res II* 44(5):1109–1128
- van der Gaast SJ, Jansen JHF (1984) Mineralogy, opal, and manganese of middle and late quaternary sediments of the Zaire (Congo) deep-sea fan: origin and climatic variation. *Neth J Sea Res* 17:313–341
- Wagner T, Zabel M, Dupont L, Holtvoeth J, Schubert CJ (2004) Terrigenous signals in sediments of the low latitude Atlantic: implications for environmental variations during the late Quaternary. Part I. Organic carbon. In: Wefer G, Mulitza S, Rathmeyer V (eds) *The South Atlantic in the late Quaternary: reconstruction of material budget and current systems*. Springer, Berlin, pp 295–322
- Wefer G, Fischer G (1993) Seasonal patterns of vertical particle flux in equatorial and coastal upwelling areas of the eastern Atlantic. *Deep-Sea Res I* 40(8):1613–1645
- Wenzhoefer F (1999) Biogeochemical processes at the sediment water interface and a quantification of metabolically driven calcite dissolution in deep-sea sediments. Universität Bremen Ber Fachbereich Geowiss 138
- Wenzhoefer F, Glud R (2002) Benthic carbon mineralization in the Atlantic: a synthesis based on in situ data from the last decade. *Deep-Sea Res I* 49(7):1255–1279
- Wenzhoefer F, Adler M, Kohls O, Hensen C, Strotmann B, Boehme S, Schulz HD (2001) Calcite dissolution driven by benthic mineralization in the deep sea—in situ measurements of  $\text{Ca}^{2+}$ , pH,  $\text{pCO}_2$ ,  $\text{O}_2$ . *Geochim Cosmochim Acta* 65:2677–2690
- Wollast R (1998) Evaluation and comparison of the global carbon cycle in the coastal zone and in the open ocean. In: Brink KH, Robinson AR (eds) *The Sea*, vol 10. Wiley, New York, pp 213–252
- Zabel M, Dahmke A, Schulz HD (1998) Regional distribution of phosphate and silicon fluxes across the sediment water interface in the eastern South Atlantic. *Deep-Sea Res I* 45(2/3):277–300